Communications in Physics, Vol. 33, No. 3 (2023), pp. 285-296
DOI: https://doi.org/10.15625/0868-3166/17642

Effect of dipolar interaction on magnetic properties of magnetite nanoparticles system

N T. Hoang[1,2,†], **T. N. Lan**[3] **and N. M. Tuan**[4]

[1]*Ho Chi Minh city Institute of Physics, National Institute of Applied Mechanics and Informatics, Vietnam Academy of Science and Technology, 1 Mac Dinh Chi, District 1, Ho Chi Minh city, Vietnam*

[2]*Graduate University of Science and Technology, Vietnam Academy of Science and Technology, 18 Hoang Quoc Viet, Cau Giay, Hanoi, Vietnam*

[3]*Department of Physics, International University, Vietnam National University Ho Chi Minh city, Quarter 6, Linh Trung Ward, Thu Duc District, Ho Chi Minh city, Vietnam*

[4]*Institute of Applied Materials Science, Vietnam Academy of Science and Technology, 1B TL29, District 12, Ho Chi Minh city, Vietnam*

E-mail: †nthoang@hcmip.vast.vn

Received 9 November 2022; *Accepted for publication 3 May 2023*; *Published 12 August 2023*

Abstract. *Magnetite nanoparticles are potential candidates for novel applications. The inter-particle interactions play a significant role in determining the overall magnetic behavior of magnetic nanoparticle assembly, especially in the case of dipolar interactions. In this paper, we have synthesized a sample and applied an atomistic spin model simulation study with input parameters obtained from experimental measurements to investigate the influence of the dipolar interaction on the magnetic properties of Fe_3O_4 magnetite nanoparticles. The results show that the dipolar interaction has certain effects on the magnetic behavior of the magnetite nanoparticles ensemble with a constant particle density. Especially when there is no magnetic field, the dipolar interaction affects the relaxation time of the magnetic moments, which leads to the interruption of thermal fluctuations, thereby reducing the magnetization of the MNPs system.*

Keywords: atomistic spin model simulation; magnetite nanoparticle; inter-particle interaction; dipolar interaction.

Classification numbers: 75.75.Fk; 88.10.gc.

1. Introduction

Over the last decade, Fe_3O_4 magnetite nanoparticles (MNPs) have demonstrated huge potential in various fields of application such as magnetic storage media [1], magnetic sensors [2],

catalysis [3], and particularly bioapplications. They have been extensively researched for emerging applications such as magnetic resonance imaging (MRI) contrast agents [4], hyperthermia therapy [5], and targeted drug delivery systems (TDDS) [6]. The MNPs have many advantages such as low toxicity, biocompatibility, easily embedded inside biodegradable polymers. Therefore, they became one of the most common magnetic nanomaterials in the fully promising bioapplications mentioned above.

The magnetic properties of MNPs would affect the performance as well as the effectiveness of the applications. Many factors determine the magnetic properties of an MNPs system that have been studied previously such as particle size [7, 8], coating layer [9–13], and inter-particle interactions [14–19]. In inter-particle interactions, dipolar interactions affect to agglomeration of the MNPs system which forms clusters or chains [20]. That has led to nanoparticle concentrations being inhomogeneous in biological systems [21]. Thence, the dipolar interaction plays a pivotal role in heat-delivery applications that affect heating efficiency for hyperthermia applications in cancer treatment. Ferromagnetic resonance (FMR) spectroscopic technique could be applied to investigate the dipolar interactions among the MNPs [22, 23]. However, the analysis of FMR results is complicated. On one hand, in experimental process, the elimination of the effects of thermal relaxation of MNPs system is possible by performing the measurement at low temperatures. On the other hand, it is impossible to eliminate the dipole interaction between the MNPs. Therefore, we can quantify the dipole field as well as the dipolar interaction but showing the effect of the dipolar interaction on the magnetic properties of the MNPs is a challenge [20, 24, 25]. However, computer simulation approaches can solve this problem. Schmool *et al*. have performed FMR experiments on the γ-Fe_2O_3 nanoparticle system (varying sizes and densities of particles) and then presented a computer simulation investigation with a matrix of nanoparticles generated randomly [26]. The obtained results showed that the dipolar interaction plays a significant role in the shaping of magnetic properties of the magnetic nanoparticle system. The study concluded that the spatial distribution and the density of particles would affect the dipolar interaction which determines the magnetic behavior of the nanoparticles system. Though, it does not explicitly state how the effect of the dipolar interaction on the magnetic properties of the nanoparticle system. Recently, Fabris *et al*. have developed a random anisotropy model by mean field theory to describe the magnetization curve of MNPs embedded inside paraffin [27]. This method has provided a new model which allows quantitative description of the effect of the dipolar interaction between MNPs, and the results are in good agreement with the experiment. Nevertheless, in this case, the MNPs are immobilized in the matrix of paraffin that affects the distribution and density of the particles in particular and the magnetic properties of the particle system in general. Therefore, it is impossible to accurately indicate the effect of the dipolar interaction on the magnetism characterization of the MNPs system.

In the present paper, we fabricate a bare MNPs system, then measure the characteristics of the synthesized sample by experimental methods such as X-ray diffraction (XRD), Transmission Electron Microscopy (TEM), and Vibrating Sample magnetometer (VSM). Finally, these results are brought into the input parameters for the computer simulations. By this method, we try to best simulate a practical MNPs system to ensure the accuracy in computer simulations. The atomistic spin model simulation of magnetic nanomaterials supplies detail about the fundamental physical processes that govern their macroscopic properties and allows the simulation of complex effects

like inter-particle interactions. Regarding the simulation process, we use the VAMPIRE software [28], which is an open-source package distributed by University of York (United Kingdom). It is not only available with different methods to perform an atomistic spin model simulation for magnetic materials like Monte Carlo integration [29], Landau-Lifshitz-Gilbert (LLG) [30], Heisenberg mean-field theory [31] but also provides the ability to accurately compute the dipolar interaction using two methods: macrocell approximation [32] and tensor approach [33], the latter is faster than the former. Previous studies have demonstrated that the LLG-Heun method is suitable for magnetic dynamic systems with evolution in time [34, 35]. Thus, this work focuses on using the LLG-Heun method and the tensor approach to study the Zero Field Cooled (ZFC) and Field Cooled (FC) magnetization curves and the hysteresis loop of MNPs, which enable to investigate the effect of dipolar interaction on the magnetic properties of MNPs. The simulation results will be compared with the experimental results to ensure the accuracy of the atomistic spin model simulation.

2. Methods

2.1. Experiment

In this work, the practical MNPs clusters are fabricated using the co-precipitation method, which is one of most popular and convenient methods not only in the laboratory but also on the industrial scale. Details of the sample preparation have been reported in our previous studies [36] and other literatures [37–39]. Alternatively, we can also use commercially available versions of Fe_3O_4 magnetic nanoparticles to save time.

The synthesized sample is characterized by analytical techniques such as the XRD to determine the phase composition, and the TEM image to determine the physical size of the MNPs. In addition, VSM quantifies important magnetic parameters and investigates the magnetization behavior of the MNPs system at room temperature. These results provide input parameters for the atomistic simulations presented below.

2.2. Theoretical model and computer simulation

Here we describe the two major theories used in our computer simulation: the atomistic spin model and LLG integration.

Computer simulations are carried out using an atomistic spin model which is the fundamental framework for VAMPIRE software working. The energy of the MNPs system is generally described in terms of the Hamiltonian H as the sum of all energy contributions. The four most significant contributors include the exchange interaction between pairs of local spins (H_{exc}), the magnetic uniaxial anisotropy (H_{ani}), the applied external magnetic field (H_{app}), and the dipolar field (H_{dip}). Typical Heisenberg-type spin Hamiltonian employed in the calculations are given as follows:

$$H = H_{exc} + H_{ani} + H_{app} + H_{dip}, \tag{1}$$

$$H = -\sum_{i \neq j} J_{ij} S_i . S_j - k_{eff} \sum_i (S_i . e)^2 - \sum_i \mu_s S_i . B + \frac{\mu_0 \mu_s}{4\pi r_{ij}^3} \left[S_i . S_i - \frac{3}{{r_{ij}}^3} (S_i . r_{ij})(S_j . r_{ij}) \right], \tag{2}$$

where J_{ij} describes the contributions of exchange interaction between magnetic moments i and j of the nearest neighbors, S_i and S_j is a unit vector denoting the local spin moment direction.

Besides, k_{eff} is the effective anisotropy energy per atom, $k_{\text{eff}} = K_{\text{eff}}.a^3/n_{\text{at}}$, where K_{eff} is effective anisotropy energy, a is size of system and n_{at} is number of atoms. Meanwhile, μ_s is atomic magnetic moment, B is the external applied field. Finally, r_{ij} is distance between spins i and j, μ_0 is vacuum permeability and μ_s is the local spin moment.

The Hamiltonian can describe the energy of the MNPs system but does not give information about the dynamics of the spin. To tackle this issue, the atomistic LLG equation is used to govern the dynamic behavior of spin and is given by:

$$\frac{\partial S_i}{\partial t} = -\frac{\gamma}{(1+\lambda^2)}\left[S_i \times H^i_{eff} + \lambda S_i \times \left(S_i \times H^i_{eff}\right)\right], \tag{3}$$

where λ is the phenomenological damping parameter (Gilbert damping parameter) which is an intrinsic property of the magnetic material. Meanwhile, γ is the gyromagnetic ratio and H^i_{eff} is the net effective magnetic field on each spin. The H^i_{eff} is given by:

$$H^i_{eff} = -\frac{1}{\mu_z}\frac{\partial H}{\partial S_i} + H^i_{th}. \tag{4}$$

The thermal fluctuations are represented by a Gaussian distribution in three dimensions with a mean of zero. At each time step the instantaneous thermal field on each spin i is given by:

$$H^i_{th} = \Gamma(t)\sqrt{\frac{2\lambda k_B T}{\gamma \mu_s \Delta t}}, \tag{5}$$

where k_B is the Boltzmann constant, T is the system temperature and Δt is the integration time step.

The LLG equation is integrated numerically using the Heun numerical scheme, which becomes the LLG-Heun method in VAMPIRE software [40]. It is a feasible method of integration to simulate the evolution of spin dynamics. That allows the implementation of the magnetization curve simulations of the MNPs.

During the simulations process, a random matrix of MNPs is generated (system size is 200 nm $\times$ 200 nm $\times$ 17 nm), the particle size of MNPs is taken from our experimental result, the spacing between the particles is kept constant at 4 nm for optimization calculation results and the effective anisotropy constant $K_{\text{eff}} = 15(kJ/m^3)$ [41]. Besides, the magnetization quantities are expressed as normalized magnetization $(m = M/M_s)$, where M_S is the saturation magnetization and M is the magnetization of the MNPs system. Computer simulations in this work use parallel computing architectures (based on Message Passing Interface - MPI) on four nodes (20 cores per node) to accelerate computational simulations.

3. Results and discussion

3.1. Experimental results

X-ray diffraction

The phase formation of the samples was analyzed by XRD patterns, obtained with the D8 Advance – Brucker diffractometer (Germany), using CuK_α radiation with $\lambda = 0.15406$ nm) in the range of 2θ from 10° to 70° at room temperature (300 K).

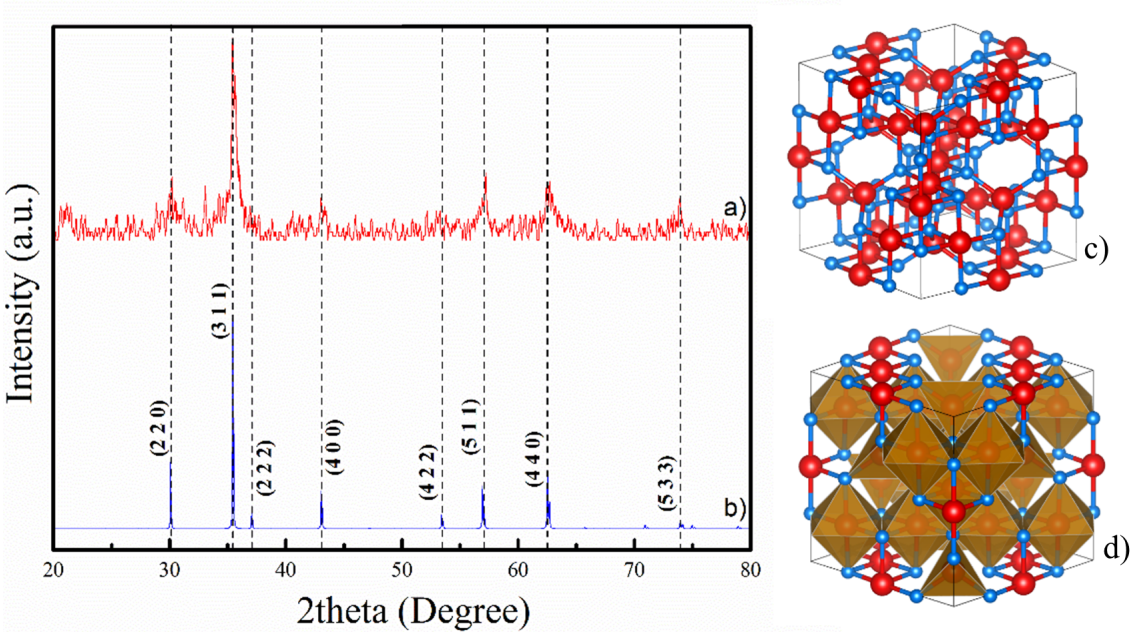

Fig. 1. X-ray diffraction pattern of (a) the synthesized Fe_3O_4 MNPs, (b) Fe_3O_4 standard pattern, (c) unit cell of Fe_3O_4, (d) Polyhedral unit cell of Fe_3O_4.

Figure 1 shows the XRD pattern of synthesized bare Fe_3O_4 MNPs (Figure 1a). According to X-ray diffraction analysis (Fig. 1a), the diffraction peaks at lattice planes (2 2 0), (3 1 1), (4 0 0), (4 2 2), (5 1 1) and (4 4 0) are well matched with the standard XRD data for magnetite (JCPDS cards No.75-0033) (Fig. 1b). It was observed that there is only one physical phase due to the presence of magnetite. In addition, no any other diffraction peaks corresponding to ferric chloride or other iron oxide, such as Fe_2O_3, was detected. This reveals that the resultant particles are mainly pure Fe_3O_4 MNPs of the face-centered cubic (FCC) crystal structure. Similar result has also been reported by other studies [42].

The Scherrer equation was used for obtaining the average crystallite sizes (d_{XRD}) of the samples:

$$d_{XRD} = \frac{K.\lambda}{\beta.\cos\theta}, \tag{6}$$

where $K \approx 0.9$ is the Scherrer constant, β is the full width at half maxima of the strongest intensity diffraction peak, λ is the wavelength of radiation and θ is the angle of the strongest peak. The obtained average crystallite size of the Fe_3O_4 MNPs is $d_{Fe_3O_4} = 15.8$ (nm).

Microstructure and morphology

In order to determine the particle size distribution and morphology of the synthesized material Transmission electron microscopy (TEM, JEM-2100) at a voltage of 100 kV was carried out. The particle size distribution of the MNPs was determined by measuring the diameter of 100 particles from the TEM images, sorting the sizes into a histogram. Then fitting the histogram data

to a log-normal function:

$$f(D) = \frac{1}{\sqrt{2\pi}\sigma D} exp\left[\frac{-\ln^2(D/D_0)}{2\sigma^2}\right], \tag{7}$$

where D_0 is the most probable particle diameter and σ is the width of the distribution. The median diameter $\langle D_{TEM}\rangle = D_0 \cdot \exp\left(\sigma^2/2\right)$ and standard deviation of the distribution $\sigma_{TEM} = \langle D_{TEM}\rangle \cdot \left[\exp\left(\sigma^2\right) - 1\right]^{1/2}$.

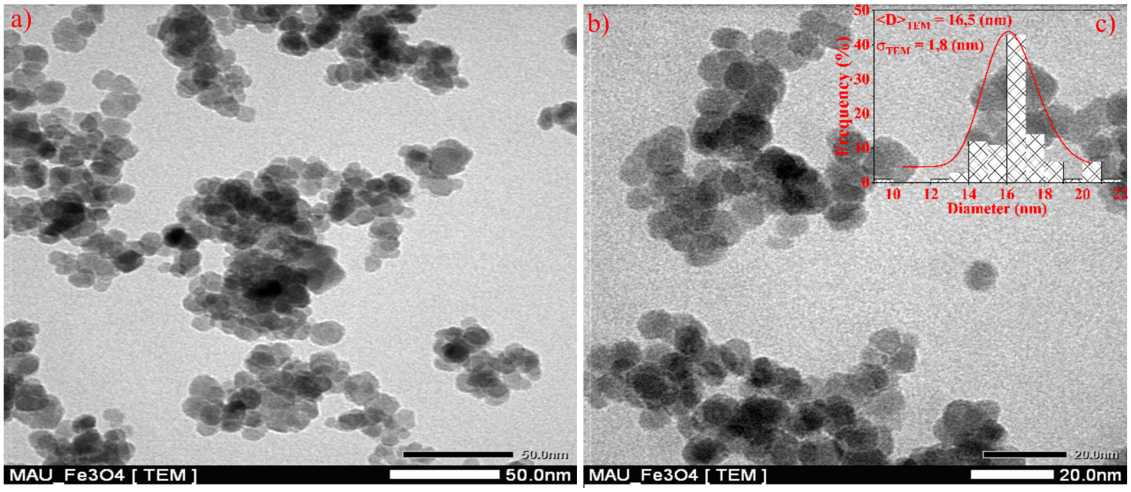

Fig. 2. TEM images of the MNPs at two scales: a) 50 nm, b) 20 nm, c) Histogram of particle size distribution fitted with a log-normal function (bold solid lines)

The TEM images of the Fe_3O_4 MNPs in Figure 2 show that the samples consist of particles with a nearly spherical shape and are quite uniform in size. The median size was $\langle D\rangle_{TEM}$ = 16.5 (nm), the corresponding standard deviation σ_{TEM} = 1.8 (nm). The TEM size is in good agreement with the one obtained from XRD pattern. This obtained result will be used in the simulations presented below.

Magnetic properties

VSM (MicroSense USA-Model 029349-A01 6MM) was used to analyze the fundamental magnetic properties of the synthesized sample at room temperature (300 K). A magnetic field of amplitude up to 15 kOe (1.19×10^6 A.m^{-1}) was applied.

Figure 3 displays the magnetization curve of MNPs, the results show that saturation magnetization M_s= 42.2 (emu/g), remnant magnetization M_r = 2.7 (emu/g), and coercive field H_c= 32.2 (Oe). When comparing with the results obtained from other recent report, e.g. [38], although our magnetization saturation is smaller (42.2 <88.1 emu/g), the remnant magnetization and coercive field are much smaller. This is beneficial for biomedical applications. We can notice there is a difference in the particle size of MNPs, the fabricated sample by Walid M Daoush *et al.* is approximately 30 nm in size which is much larger than the size obtained by our TEM observation (~16.5 nm). Meanwhile, similar results to ours were also reported by Petcharoen *et al.* [39].

As mentioned before, the major reason for the variety is due to the particle size dependence of magnetic properties of MNPs [7, 8].

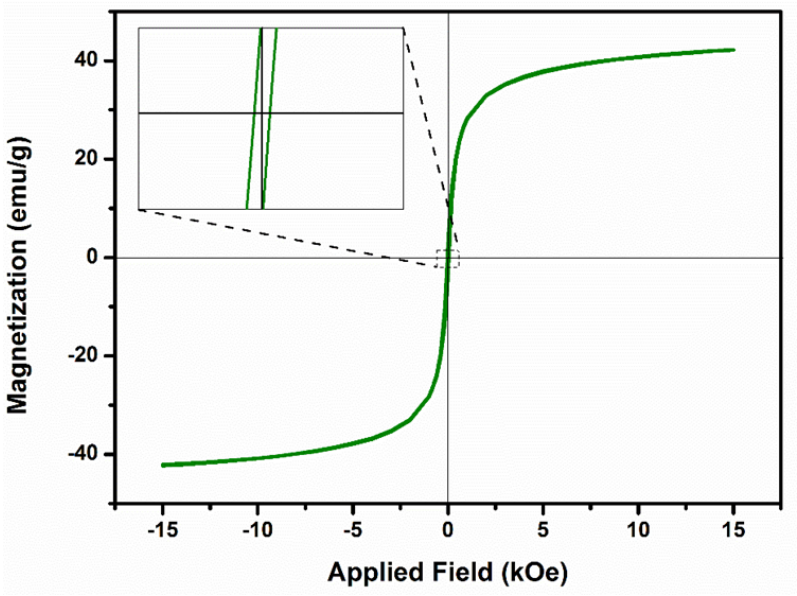

Fig. 3. The magnetization curve of the MNPs at room temperature.

3.2. Computer simulation results

Hysteresis loops

Hysteresis loop simulations are performed at absolute zero temperature to eliminate thermal relaxation phenomena of the MNPs system [43, 44]. Moreover, the dipolar interaction presence among particles in the MNPs system is determined by the value of H_{dip} in Eq. (1) which is zero/non-zero for the OFF/ON state of the dipolar interaction, respectively. That allows intuitive investigation of the effect of the dipolar interaction on the hysteresis curve of the MNPs system.

Figure 4 shows the difference clearly between the two states exists/not exists of the dipolar interaction (Dipolar ON/Dipolar OFF). Specifically, when the dipolar interaction does not exist, the remnant magnetization and coercive field of the MNPs system reaches the maximum and is much larger than when the dipolar interaction exists. In addition, at the dipolar OFF state, the magnetization reaches its maximum value (saturation) even in zero external magnetic fields $(H = 0)$. The reason is that the magnetic moments of the MNPs at absolute zero are "frozen", the difference in energy barrier height between the states becomes significant, so they are blocked in stable configurations other than the lowest-energy configuration, it has led to the magnetization growing monotonically [44, 45]. Meanwhile, in the Dipolar ON state, the magnetization reaches saturation at 0.25 (T) magnetic field. It proves that the dipolar interaction has affected the hysteresis loops of the MNPs system, which reduces the remnant magnetization and coercive field. We can explain this as follows: at absolute zero there does not exist thermal relaxation, a contribution

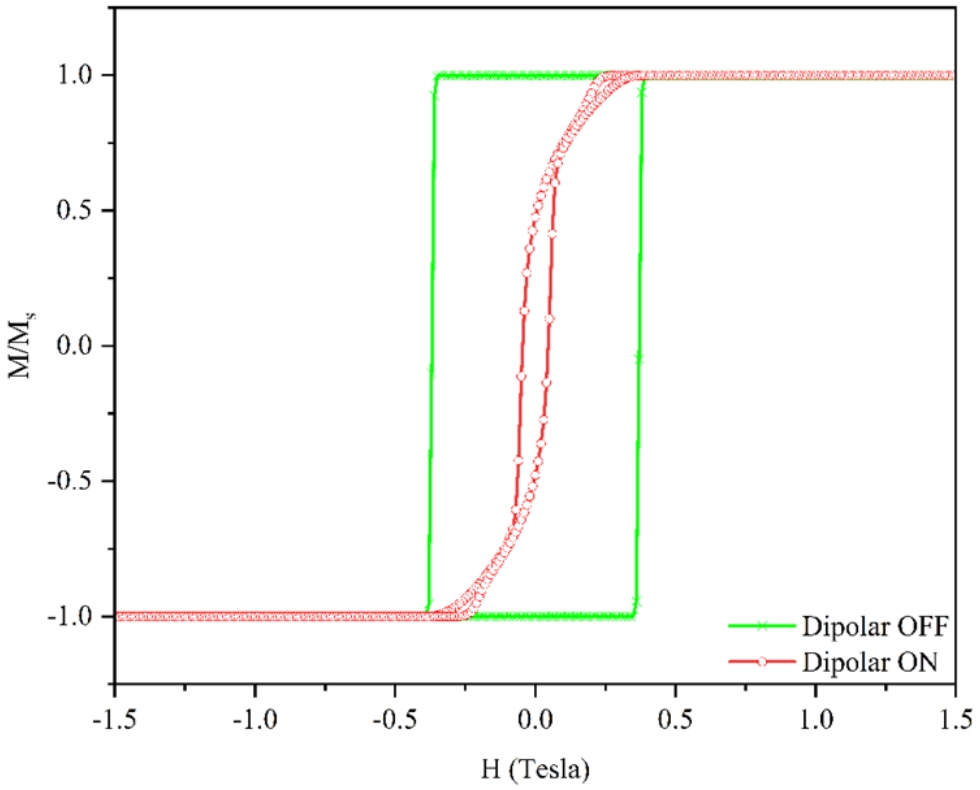

Fig. 4. The simulation results of hysteresis loop curve of the MNPs systems at 0 K.

of the dipole field among the magnetic spins of the particles becomes significant in internal energy at a low external magnetic field. This effects on the relaxation time of magnetic moment so makes them fluctuate [46]. Therefore, the particles localized at the potential well of the stable state will receive enough energy to overcome the barrier to transition to another state. Finally, the spontaneous magnetization of the MNPs system is reduced.

ZFC/FC magnetization curves

Figure 5 shows the simulated ZFC/FC magnetization curve of the MNPs system in two states: Dipole OFF and ON. A weak magnetic field (H ~ 0.005 T = 50 Oe) and no external magnetic field are applied to obtain the FC and ZFC magnetization curves, respectively. Observing these M(T) thermal magnetization curves, we notice that they converge at a temperature of ~860 (K) which is the Curie temperature of the Fe_3O_4 magnetite material. Many previously reported experimental studies are concordant with this [47–49] which represents a high agreement between the computer simulations in this work and the practical experimental results.

Examination of the effects of the dipolar interactions by investigating ZFC/FC magnetization curves obtained from standard experimental protocols indicates no dramatic change in these quantities [25]. However, the ZFC/FC magnetization curves simulated in this work show unambiguous change. On the one hand, for the FC magnetization curves, the dipolar interaction does

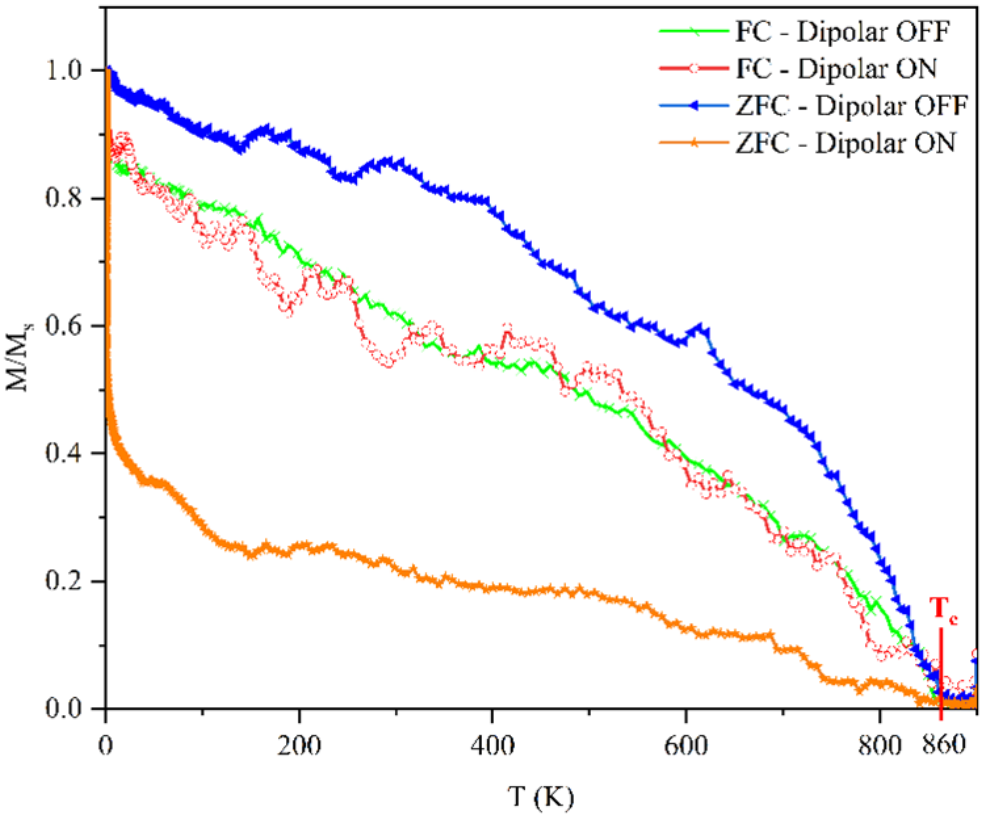

Fig. 5. The simulation results of ZFC/FC magnetization curves of the MNPs systems.

not have a significant influence in the high-temperature region (above 600 K). However, it reduces the magnetization in the vicinity of the Curie temperature. The reason is that the magnetic spins fluctuate freely by thermal effect. In addition, the contribution of the dipolar interaction to the intrinsic energy of the MNPs system has led to the magnetic spin configuration of the particles being further perturbed, thereby reducing the magnetization. Besides that, at the intermediate temperatures (50-550 K), where the relaxation time of a spin is comparable to the observation time, dynamical magnetic relaxation can be observed explicitly. At low temperatures (0-50 K), due to spin-glass transition [25, 43, 45], the magnetic moment is in blocked state, so the effect of dipole interactions becomes secondary.

On the other hand, the ZFC magnetization curves explicitly display the change between the two states ON/OFF of the dipolar interaction. In the Dipolar ON state, the magnetization is strongly reduced compared to the Dipolar OFF state. The reason is that when the applied magnetic field is zero, the dipolar interaction affects the relaxation time of the magnetic moments [46], which leads to the interruption of thermal fluctuations, thereby reducing the magnetization of the MNPs system (Fig. 6a). The same as above, the magnetic moment is blocked at approximately absolute zero with their parallel orientation (Fig. 6b), the effect of dipolar interaction is not enough to unblock them. As a result, the magnetization reaches a maximum.

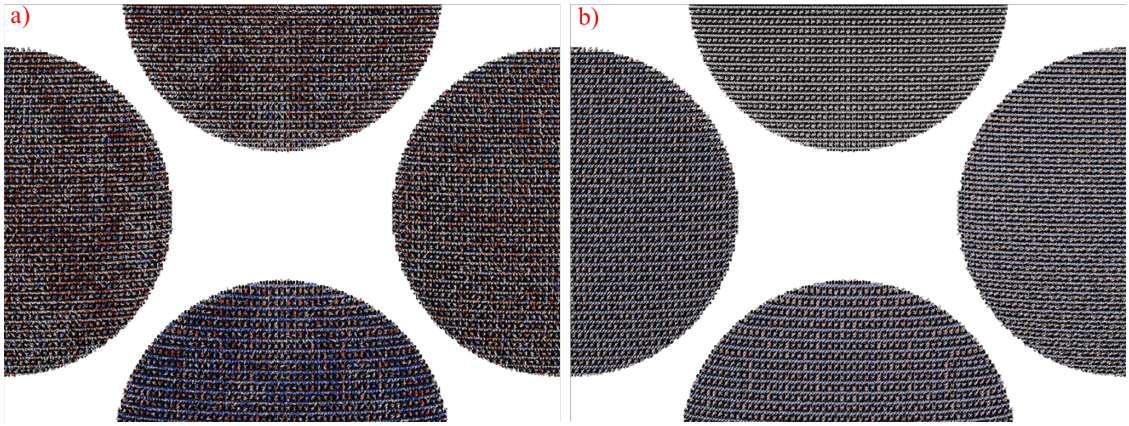

Fig. 6. Snapshots of the MNPs during ZFC magnetization curves simulations at high and intermediate temperatures (a) and low temperature (b).

4. Conclusions

In this work, the purified Fe_3O_4 MNPs were synthesized to have a monocrystalline structure, single domain. Then it was characterized by some standard experimental protocols. These practical results provide the input parameters for the computer simulations based on the atomistic spin model. The LLG-Heun method was applied to simulate the magnetic dynamic behavior, while the tensor approach allows the calculation of the dipolar interactions of the magnetic nanoparticles. Simulating and investigating the hysteresis loops and ZFC/FC magnetization curves of the MNPs system, we have provided a simple method, probably too rough to well account for the role and influence of dipolar interactions on the physical magnetic properties of the practical MNPs system. Finally, we will evoke some unsolved issues, variation of different concentrations of the MNPs system is not yet assessed. That will also contribute to determining the influence of dipole interactions on the magnetic properties of the MNPs system. Many studies remain to do.

Acknowledgment

Financial support of the Vietnam Academy of Science and Technology (VAST) via the project ĐLTE00.02/22-23 is gratefully acknowledged. The computer simulations for this work were undertaken on the HPC01 Cluster and HCMIP Cluster, which are high-performance computing facilities provided by the Center Informatics and Computing - VAST and Ho Chi Minh City Institute of Physics - VAST, respectively. We would like to thank the HCMIP research computing team for support from their computing service.

References

[1] S. Jamil and M. R. S. A. Janjua, *Synthetic study and merits of Fe_3O_4 nanoparticles as emerging material*, J. Clust. Sci. **28** (2017) 2369.

[2] A. G. Kolhatkar, Y.-T. Chen, P. Chinwangso, I. Nekrashevich, G. C. Dannangoda, A. Singh *et al.*, *Magnetic sensing potential of Fe_3O_4 nanocubes exceeds that of Fe_3O_4 nanospheres*, ACS Omega **2** (2017) 8010.

[3] M. A. E. A. A. A. El-Remaily, *Synthesis of pyranopyrazoles using magnetic Fe_3O_4 nanoparticles as efficient and reusable catalyst*, Tetrahedron **70** (2014) 2971.

[4] S. Arsalani, E. J. Guidelli, M. A. Silveira, C. E. Salmon, J. F. Araujo, A. C. Bruno *et al.*, *Magnetic Fe_3O_4 nanoparticles coated by natural rubber latex as MRI contrast agent*, J. Magn. Magn. Mater. **475** (2019) 458.

[5] S. L. Gawali, S. B. Shelar, J. Gupta, K. C. Barick and P. A. Hassan, *Immobilization of protein on Fe_3O_4 nanoparticles for magnetic hyperthermia application*, Int. J. Biol. Macromol. **166** (2021) 851.

[6] Y. Y. Pin, K. Shameli, M. Miyake, N. B. B. A. Khairudin, S. E. B. Mohamad, T. Naiki *et al.*, *Green biosynthesis of superparamagnetic magnetite Fe_3O_4 nanoparticles and biomedical applications in targeted anticancer drug delivery system: A review*, Arab. J. Chem. **13** (2020) 2287.

[7] V. Patsula, M. Moskvin, S. Dutz and D. Horák, *Size-dependent magnetic properties of iron oxide nanoparticles*, J. Phys. Chem. Solids **88** (2016) 24.

[8] J. Chatterjee, Y. Haik and C.-J. Chen, *Size dependent magnetic properties of iron oxide nanoparticles*, J. Magn. Magn. Mater. **257** (2003) 113.

[9] Y. Yuan, D. Rende, C. L. Altan, S. Bucak, R. Ozisik and D.-A. Borca-Tasciuc, *Effect of surface modification on magnetization of iron oxide nanoparticle colloids*, Langmuir **28** (2012) 13051.

[10] I. M. Lourenço, M. T. Pelegrino, J. C. Pieretti, G. P. Andrade, G Cerchiaro and A. B. Seabra, *Synthesis, characterization and cytotoxicity of chitosan-coated Fe_3O_4 nanoparticles functionalized with ascorbic acid for biomedical applications*, J. Phys. Conf. Ser. **1323** (2019) 012015.

[11] H. K. Can, S. Kavlak, S. ParviziKhosroshahi and A. Güner, *Preparation, characterization and dynamical mechanical properties of dextran-coated iron oxide nanoparticles (DIONPs)*, Artif. Cells Nanomed. Biotechnol. **46** (2018) 421.

[12] R. Gupta, K. Pancholi, R. D. Sa, D. Murray, D. Huo, G. Droubi *et al.*, *Effect of oleic acid coating of iron oxide nanoparticles on properties of magnetic polyamide-6 nanocomposite*, JOM **71** (2019) 3119.

[13] S. Larumbe, C. Gomez-Polo, J. I. Pérez-Landazábal and J. M. Pastor, *Effect of a SiO_2 coating on the magnetic properties of Fe_3O_4 nanoparticles*, J. Phys.: Condens. Matter **24** (2012) 266007.

[14] R. T. Reza, C. A. M. Pérez, C. A. R. González, H. M. Romero and P. E. G. Casillas, *Effect of the polymeric coating over Fe_3O_4 particles used for magnetic separation*, Open Chem. **8** (2010) 1041.

[15] V. Sreeja and P. A. Joy, *Effect of inter-particle interactions on the magnetic properties of magnetite nanoparticles after coating with dextran*, Int. J. Nanotechnol. **8** (2011) 907.

[16] A. F. Abu-Bakr and A. Zubarev, *Effect of interparticle interaction on magnetic hyperthermia: homogeneous spatial distribution of the particles*, Phil. Trans. R. Soc. A. **377** (2019) 20180216.

[17] P. E Jönsson, *Effects of interparticle interaction in ferromagnetic nanoparticle systems*, J. Nanosci. Nanotechnol. **10** (2010) 6067.

[18] E. Lima, J. M. Vargas, H. R. Rechenberg and R. D. Zysler, *Interparticle interactions effects on the magnetic order in surface of Fe_3O_4 nanoparticles*, J. Nanosci. Nanotechnol. **8** (2008) 5913.

[19] B. Aslibeiki, M. H. Ehsani, F. Nasirzadeh and M. A. Mohammadi, *The effect of interparticle interactions on spin glass and hyperthermia properties of Fe_3O_4 nanoparticles*, Mater. Res. Express **4** (2017) 075051.

[20] L. Gutiérrez, L. de la Cueva, M. Moros, E. Mazarío, S. de Bernardo, J. M de la Fuente *et al.*, *Aggregation effects on the magnetic properties of iron oxide colloids*, Nanotechnol. **30** (2019) 112001.

[21] L. C. Branquinho, M. S. Carrião, A. S. Costa, N. Zufelato, M. H. Sousa, R. Miotto *et al.*, *Effect of magnetic dipolar interactions on nanoparticle heating efficiency: Implications for cancer hyperthermia*, Sci. Rep. **3** (2013) 2887.

[22] J. Dubreuil and J. S. Bobowski, *Ferromagnetic resonance in the complex permeability of an Fe_3O_4-based ferrofluid at radio and microwave frequencies*, J. Magn. Magn. Mater. **489** (2019) 165387.

[23] A. S. Vakula, A. G. Belous, T. V. Kalmykova, S. I. Petrushenko, V. N. Sukhov and S. I. Tarapov, *Ferromagnetic resonance in the complex of Fe_3O_4 nanoparticles with organic compounds*, Telecommun. Radio Eng. **77** (2018) 257.

[24] E. Myrovali, K. Papadopoulos, I. Iglesias, M. Spasova, M. Farle, U. Wiedwald *et al.*, *Long-range ordering effects in magnetic nanoparticles*, ACS Appl. Mater. Interfaces **13** (2021) 21602.

[25] P. E Jönsson, *Superparamagnetism and spin glass dynamics of interacting magnetic nanoparticle systems*, Adv. Chem. Phys. **128** (2003) 191.

[26] D. S. Schmool and M. Schmalzl, *Magnetic dipolar interactions in nanoparticle systems: theory, simulations and ferromagnetic resonance*, Adv. Nanoscale Magn. **122** (2009) 321.

[27] F. Fabris, Kun-Hua Tu, C. A. Ross and W. C. Nunes. *Influence of dipolar interactions on the magnetic properties of superparamagnetic particle systems*, J. App. Phys. **126** (2019) 173905.
[28] R. F. L. Evans, W. J. Fan, P. Chureemart, T. A. Ostler, M. O. A. Ellis *et al.*, *Atomistic spin model simulations of magnetic nanomaterials*, J. Phys.: Condens. Matter **26** (2014) 103202.
[29] J. E. Gubernatis, *Marshall Rosenbluth and the Metropolis algorithm*, Phys. Plasmas **12** (2005) 057303.
[30] T. L. Gilbert, *A Lagrangian formulation of the gyromagnetic equation of the magnetization field*, Phys. Rev. **100** (1955) 1243.
[31] R. F. L. Evans, L. Rózsa, S. Jenkins and U. Atxitia, *Temperature scaling of two-ion anisotropy in pure and mixed anisotropy systems*, Phys. Rev. B **102** (2020) 020412.
[32] G. Bowden, G. Stenning and G. Laan, *Inter and intra macro-cell model for point dipole–dipole energy calculations*, J. Phys.: Conden. Matter **28** (2016) 066001.
[33] H. Zhi, T. Ma, D. Pei and H. Sun, *A novel magnetic dipole inversion method based on tensor geometric invariants*, AIP Advances **10** (2020) 045131.
[34] F. Schlickeiser, *Multi-scale modeling of the thermal control of magnetic nanostructures*, PhD Thesis, University of Konstanz, 2016.
[35] D. Arjmand, M. Poluektov and G. Kreiss, *Atomistic-continuum multiscale modelling of magnetisation dynamics at non-zero temperature*, Adv Comput Math **44** (2018) 1119.
[36] H. T. Nguyen and T. M. Nguyen, *Investigation of magnetic properties of magnetic poly (glycidyl methacrylate) microspheres: experimental and theoretical*, Adv. Matter. Sci. Eng. **2021** (2021) 1.
[37] A. Chintaparthi and J. Philip, *Efficient removal of methylene blue dye using cellulose capped Fe_3O_4 nanofluids prepared using oxidation-precipitation method*, Colloids Surf. **567** (2019) 193.
[38] W. M. Daoush, *Co-precipitation and magnetic properties of magnetite nanoparticles for potential biomedical applications*, J. Nanomed. Res. **5** (2017) 00118.
[39] K. Petcharoen and A. Sirivat, *Synthesis and characterization of magnetite nanoparticles via the chemical co-precipitation method*, Mater. Sci. Eng. B. **177** (2012) 421.
[40] J. L. García-Palacios F. J. Lázaro, *Langevin-dynamics study of the dynamical properties of small magnetic particles*, Phys. Rev. B **58** (1998) 14937.
[41] H. Mamiya, H. Fukumoto, J. L. C. Huaman, K. Suzuki, H. Miyamura and J. Balachandran, *Estimation of magnetic anisotropy of individual magnetite nanoparticles for magnetic hyperthermia*, ACS Nano **14** (2020) 8421.
[42] H. Shagholani, S. M. Ghoreishi and M. Mousazadeh, *Improvement of interaction between PVA and chitosan via magnetite nanoparticles for drug delivery application*, Int. J. Biol. Macromol. **78** (2015) 130.
[43] W. Rippard, R. Heindl, M. Pufall, S. Russek and A. Kos, *Thermal relaxation rates of magnetic nanoparticles in the presence of magnetic fields and spin-transfer effects*, Phys. Rev. B **84** (2011) 064439.
[44] I. J. Bruvera, P. M. Zélis, M. P. Calatayud, G. F. Goya and F. H. Sánchez, *Determination of the blocking temperature of magnetic nanoparticles: the good, the bad, and the ugly*, J. Appl. Phys. **118** (2015) 184304.
[45] B. Martinez, X. Obradors, Ll Balcells, A. Rouanet and C. Monty, *Low temperature surface spin-glass transition in γ-Fe_2O_3 nanoparticles*, Phys. Rev. Lett. **80** (1998) 181.
[46] J. L. Dormann, *Properties of magnetically interacting small particles*, in *Magnetic properties of fine particles*, Elsevier, 1992.
[47] R. N. Panda, N. S. Gajbhiye and G. Balaji, *Magnetic properties of interacting single domain Fe_3O_4 particles*, J. Alloys Compd. **326** (2001) 50.
[48] V. N. Nikiforov, Y. A. Koksharov, S. N. Polyakov, A. P. Malakho, A. V. Volkov, M. A. Moskvina *et al.*, *Magnetism and Verwey transition in magnetite nanoparticles in thin polymer film*, J. Alloys Compd. **569** (2013) 58.
[49] P. Majewski and B. Thierry, *Functionalized magnetite nanoparticles synthesis, properties, and bioapplications*, Crit. Rev. Solid State Mater. Sci. **32** (2007) 203.